LANGMUIR Article
Cite This: Langmuir 2018, 34, 12387−12393
pubs.acs.org/Langmuir

Lipid Bilayer Disruption by Amphiphilic Janus Nanoparticles: The Role of Janus Balance

Kwahun Lee and Yan Yu*

Department of Chemistry, Indiana University, Bloomington, Indiana 47405, United States

Supporting Information

ABSTRACT: Amphiphilic nanoparticles are known to cause defects in lipid bilayers. However, we have shown recently that their disruptive effects are significantly enhanced when surface charges and hydrophobic groups are spatially segregated on opposite hemispheres of a single particle. Using the same amphiphilic cationic/hydrophobic Janus particle system, here we investigate the role of the hydrophilic−lipophilic balance of the particles (namely the Janus balance) in their interaction with zwitterionic lipid bilayers. We show that Janus nanoparticles induce holes in lipid bilayers only when the hydrophobic side of particles occupies 20% or more of their surfaces. Beyond this threshold, the larger the hydrophobic surface area, the more attractive the particles are to lipid bilayers, and a lower particle concentration is needed for causing defects in the bilayers. The results establish a quantitative relationship between the surface coverage of hydrophobicity on the Janus particles and the particle-induced disruption to the lipid membranes.

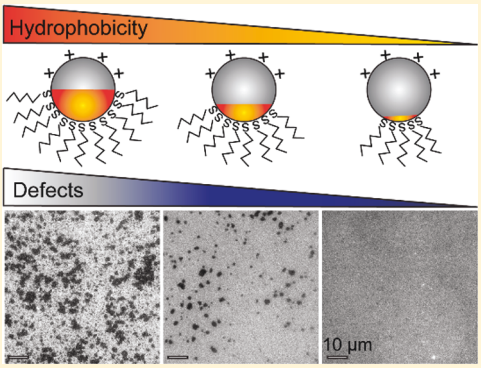

1. INTRODUCTION

Understanding the interaction of engineered nanoparticles with biological membranes is critical for assessing and predicting the potential impact of engineered nanoparticles on living systems. Extensive studies have been done to understand how these interactions are affected by the surface properties of particles. The surface properties studied include charge[1−7] and hydrophobicity.[8−11] Cationic and anionic nanoparticles have been shown to differ significantly in the way they bind to cells,[2] disrupt the integrity and function of cell plasma membranes,[1,3] enter the cell, and are transported intracellularly after entry.[4] Different surface charge effects were also observed when particles interacted with model lipid membranes.[5−7] The interaction between the membrane and the particle can become more complex when hydrophobic ligands are presented together with charges on particle surfaces. Amphiphilic particles coated with a uniform mixture of charged and hydrophobic groups have been found to induce pores in model lipid membranes[8−11] and stabilize the open edge of lipid bilayers.[12]

Most studies of the interactions between amphiphilic nanoparticles and biomembranes have focused on homogeneous particles. Only a few have investigated the effects of nonhomogeneous arrangements of ligands on the particle surface. Gold nanoparticles with striped patterns of hydrophobic and hydrophilic molecules have been shown to penetrate cell membranes more easily than the ones with random patterns.[13,14] Our group has reported recently that amphiphilic Janus nanoparticles (JPs) that are charged on one hemisphere and hydrophobic on the other induce holes in lipid bilayers.[15] Such two-faced amphiphilic nanoparticles disrupt lipid bilayers more effectively than uniformly coated particles because they can rotate to interact with the bilayer from the energetically favorable side.[15] We found in that study that the hydrophobic interaction plays a crucial role in the ability of amphiphilic Janus particles to extract lipids from intact membranes. Given the growing interest in synthesizing and using amphiphilic nanoparticles,[10,13,14,16−19] these findings are important and timely for understanding the distinctive way in which they interact with the lipid bilayer membranes. However, the mechanism by which amphiphilic particles disrupt such membranes remains poorly understood. One important question, among many, is the role hydrophobicity plays in particle−membrane interactions. For example, must particle hydrophobicity exceed some threshold for amphiphilic particles to disrupt lipid membranes? How can the effects of surface charge and particle hydrophobicity on the disruption of membranes be decoupled from one another?

Building on our recent study, here we conduct a quantitative investigation of the role of hydrophobicity in the interaction between amphiphilic JPs and zwitterionic lipid membranes. The particles were positively charged on one side and hydrophobic on the other. It is difficult to control and quantify the hydrophobicity of nanoparticles. By using the two-faced Janus particle system, we were able to fine-tune the amount of surface coverage by the hydrophobic side—the so-called Janus balance of the particle—using chemical etching. We could quantitatively measure the hydrophilic−lipophilic

Received: July 7, 2018
Revised: September 18, 2018
Published: September 21, 2018

DOI: 10.1021/acs.langmuir.8b02298
Langmuir 2018, 34, 12387−12393

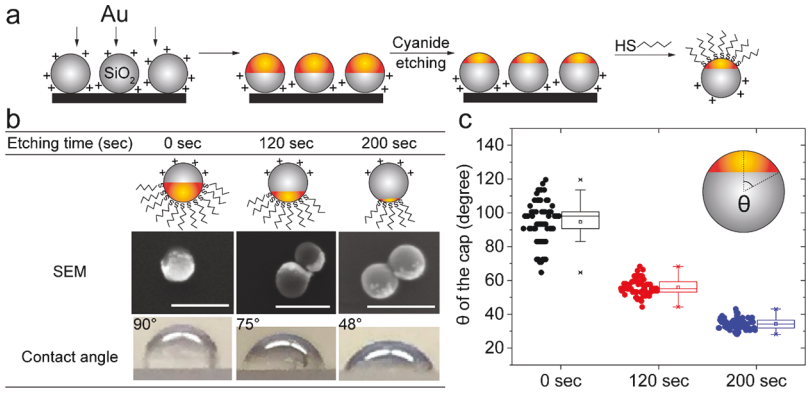

Figure 1. (a) Schematics showing the fabrication of amphiphilic Janus particles and subsequent chemical etching of the gold coating. (b) SEM and water contact angle characterization of Janus particles after various durations of etching as indicated. Scale bars: 200 nm. (c) Angle θ, as schematically illustrated in the inset, is plotted as a function of etching time. Each data point in the scattered plot represents the measurement from a single particle. Each box plot indicates the mean (squared dot), median (horizontal line), and the interquartile range from 25 to 75% of the corresponding data set.

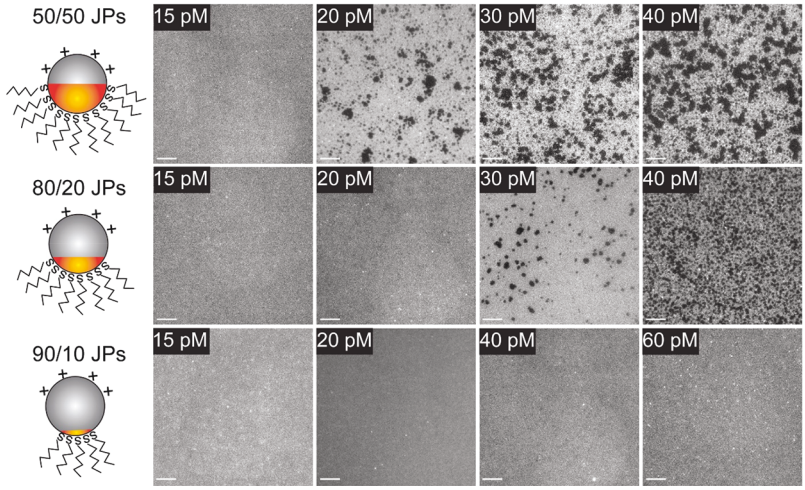

Figure 2. Fluorescence images showing the morphology of lipid bilayers after incubation with the 50/50, 80/20, and 90/10 JPs for 70 min at various particle concentrations as indicated. Each image is representative of the results from two or three independent samples. Scale bars: 10 μm.

balance of the particles. We show that the cationic/hydrophobic amphiphilic JPs induce holes in lipid bilayers when the hydrophobic side covers 20% or more of the particle surface. Beyond this threshold, more hydrophobic Janus particles are more attractive to lipid bilayers and cause defects at lower threshold concentrations. When the hydrophobic area decreases below 10% of the total particle surface, amphiphilic JPs can no longer cause any noticeable defects in bilayers. Our results reveal the exact role of hydrophobicity in the interaction between amphiphilic Janus particles and lipid membranes. More importantly, this work establishes a quantitative relationship between the hydrophobicity of amphiphilic JPs and their impact on lipid membranes.

2. RESULTS AND DISCUSSION

We fabricated 100 nm cationic/hydrophobic JPs, with controlled variations in the surface area of their hydrophobic side, using a three-step procedure. We first deposited thin films of chromium and gold on one hemisphere of amine-modified silica nanoparticles, etched the gold caps using cyanide solution, and finally conjugated hydrophobic octadecanethiol (ODT) onto the gold caps (Figure 1a). The etching was used to control the surface area of the gold cap and thus the Janus balance of the particles. The size of the remaining gold cap after etching was measured as the polar angle θ from scanning electron microscopy (SEM) images (Figures 1b and S1). The angle θ was found to decrease linearly with etching time, 55.6° ± 3.4° (avg ± SD) at 120 s and 34.2° ± 2.9° at 200 s (Figure 1b,c). For comparison, θ for nonetched Janus particles was 94.6° ± 5.1°. Correspondingly, ≈54, 22, and 9% of the particle surfaces were hydrophobic for the nonetched particles and those etched for 120 and 200 s, respectively. We therefore refer to the three types of JPs as the "50/50 JPs", "80/20 JPs", and "90/10 JPs" to reflect the different surface coverages of their hydrophobic caps. The water contact angle measured on the submonolayer of particles after the chemical etching was similar for different particles, 43° for 50/50 JPs and 40° for 90/10 JPs (Table S1, Supporting Information), but increased to ≈90°, 75°, and 48° for the 50/50, 80/20, and 90/10 JPs, respectively, after ODT conjugation (Figure 1b). This result confirms the varied hydrophobicity of the different types of Janus particles together with the remaining gold film surrounding the particles on glass substrates. It also indicates that the particle hydrophobicity is due to ODT coating, but not chemical etching. Because the cyanide solution does not etch away the chromium coating (5 nm thick) underneath the

DOI: 10.1021/acs.langmuir.8b02298
Langmuir 2018, 34, 12387−12393

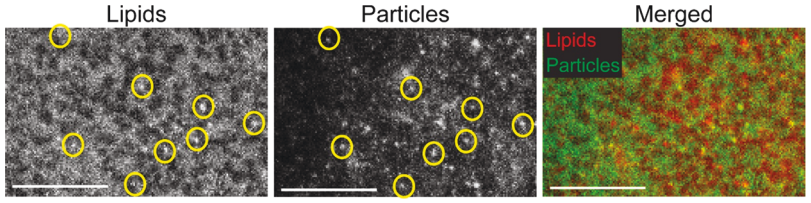

Figure 3. Fluorescence images showing the lipid bilayer (left) and 80/20 JPs (middle) after defect formation at 40 pM particle concentration. A merged image is shown on the right. The circles highlight the colocalization between the Janus particles and lipids extracted from the lipid bilayer. Scale bars: 10 μm.

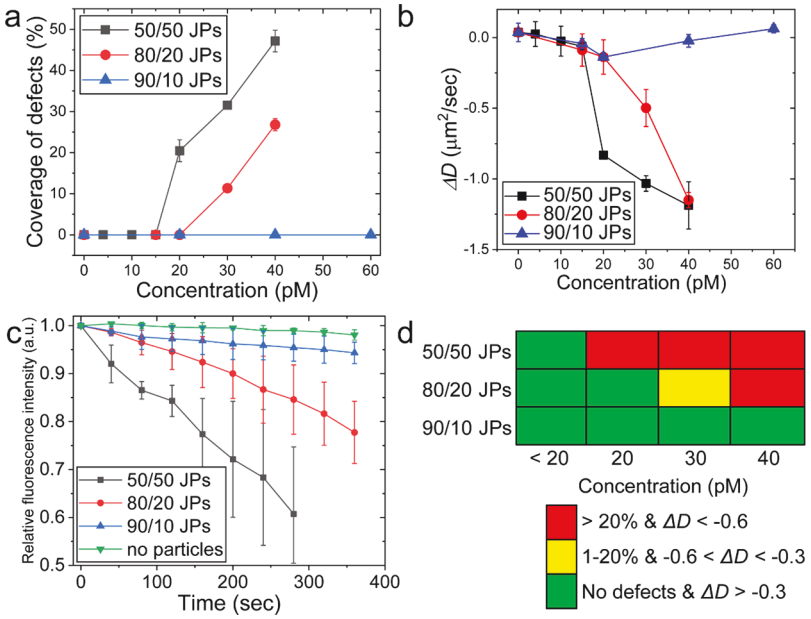

Figure 4. (a) Surface coverage of defects in lipid bilayers as a function of particle concentration for different types of Janus particles: 50/50 JPs (black squares), 80/20 JPs (red dots), and 90/10 JPs (blue triangles). (b) Change in the lipid diffusion coefficient (ΔD) after the addition of DI water (0 pM) and various concentrations of Janus particles. (c) Average fluorescence intensity of the lipid bilayer as a function of time after the addition of DI water (no particles), 90/10 JPs (blue), 70/30 JPs (red), and 50/50 JPs (black). The particle concentration was 30 pM for all three types of particles. (d) Color-coded diagram showing different effects of JPs on lipid bilayers as a function of particle hydrophobicity and particle concentration. Each data point in (a–c) is an average of the results from three independent samples. Error bars in all plots represent standard deviation.

gold layer, the surface area of the positively charged side likely remained at ≈50% for all three types of Janus particles. We assume that the chromium layer had negligible effect on the particle–membrane interaction. In ζ-potential measurements, we repeatedly observed that the ζ-potential for the amphiphilic JPs was measured negative, even though that of bare amine-modified silica nanoparticles was +25.9 mV (Table S2 of the Supporting Information). Although the exact cause for the negative ζ-potential is unclear, the measured values may not accurately reflect the surface charges on the Janus particles because the classical electrophoretic models used in ζ-potential measurements may not be applicable to metal-coated Janus particles that are known to exhibit an unusual electrokinetic motion.[20]

We next investigated the interactions between the amphiphilic JPs of varied hydrophobicity and zwitterionic lipid bilayers. The lipid bilayers were formed in deionized (DI) water on glass microscope slides by self-assembly of mostly 1,2-dioleoyl-*sn*-glycero-3-phosphocholine (DOPC) and 0.2 mol % of fluorescently labeled lipids. The morphology of the bilayers was examined using fluorescence imaging after incubation with different concentrations of JPs for 70 min (Figure 2). The 50/50 JPs at 20 and 40 pM concentrations caused large defects in the bilayers that were depleted from the lipids, as we have reported previously (Figure 2).[15] In contrast, the 80/20 JPs, with reduced hydrophobicity, only caused defects in the lipid bilayer at concentrations of 30 pM or higher. Meanwhile, lipid aggregates were also formed on bilayers, appearing as bright dots in the fluorescence images. Higher particle concentrations led to larger areas of defects and more lipid aggregates. Different from the 50/50 or 80/20 JPs, the 90/10 JPs did not cause any obvious morphological changes in the lipid bilayer even when the particle concentration was increased to 60 pM. In all experiments, we ensured that the JPs were dispersed when being added to the lipid bilayers at the concentrations shown here.

By simultaneously imaging 80/20 JPs and the lipid bilayer, we found that the lipid aggregates contained both particles and lipids (Figure 3). Most of the aggregates were distributed randomly on the bilayer, whereas some became detached. This agrees with our previous observation for 50/50 JPs and suggests that the 80/20 JPs, like the 50/50 JPs, likely extracted lipids from the bilayer onto their hydrophobic hemispheres, thereby inducing defects in the bilayers.[15] The results demonstrate that the disruptive effect of amphiphilic JPs on lipid bilayers increases as particle hydrophobicity increases.

DOI: 10.1021/acs.langmuir.8b02298
Langmuir 2018, 34, 12387–12393

However, the mechanism by which particles induce holes in lipid bilayers likely remains the same.

To quantify the disruption of lipid bilayers by particles, we measured the changes in the surface area of defects, membrane fluidity, and the time-dependent fluorescence intensity of the bilayer. The surface coverage of defects, measured as the fraction of surface area depleted from fluorescent lipids, was found to increase almost linearly with particle concentration once past the threshold for both 50/50 and 80/20 JPs (Figure 4a). In the presence of 20 pM 50/50 JPs, ≈20.5% of the bilayer was occupied by defects. This defect coverage increased to ≈31.5% at 30 pM and ≈47.2% at 40 pM. The 80/20 JPs caused defects in ≈11.3% of the bilayer surface at 30 pM and ≈26.8% at 40 pM. The fluidity of lipid bilayers is essential to their biological functions. To quantify how this fluidity is affected by amphiphilic Janus particles, we measured the ensemble-averaged diffusion coefficients of lipids using fluorescence recovery after photobleaching (FRAP) (Figure 4b). In each lipid bilayer sample, the lipid diffusion coefficient (D) was measured before and after the addition of Janus particles. The changes in lipid diffusion (ΔD) were used to indicate the change in membrane fluidity. The D value of the DOPC lipid bilayers used in this study was within the range of 1.3−1.6 $\mu m^2/s$, consistent with the previous FRAP studies of the DOPC bilayers.[21,22] The 90/10 JPs showed a negligible effect on lipid membrane fluidity. By contrast, both 50/50 and 80/20 JPs caused a drastic decrease in lipid diffusion at concentrations higher than the thresholds. The bilayer was less fluid at higher particle concentrations. Interestingly, even though the 50/50 JPs at 20 and 30 pM caused a larger decrease of bilayer fluidity compared to the 80/20 JPs, both types of particles at 40 pM resulted in nearly nonfluid bilayers with the lipid diffusion coefficients of <0.3 $\mu m^2/s$. These results indicate that the effects of both types of particles on lipid bilayers are not limited to the formation of localized holes. Their extraction of lipids also disrupts the integrity of the remaining bilayers where no defects were visible. Indeed, we found that the fluorescence intensity of the remaining lipid bilayers decreased with time in the presence of 50/50 JPs and 80/20 JPs at 30 pM (Figure 4c). The 50/50 JPs caused the most rapid decay in bilayer intensity, whereas 90/10 JPs exhibited a negligible effect. The decreased intensity of membranes further confirmed the loss of lipids from the bilayer areas without visible defects and showed that the effect of lipid extraction is stronger with more hydrophobic particles.

On the basis of the results of these measurements, we constructed a "phase" diagram to illustrate the different disruptive effects induced by amphiphilic Janus particles as a function of their hydrophobicity and concentration (Figure 4d). We categorized the results into three groups: lipid bilayers with >20% surface coverage of defects and a decrease of the lipid diffusion coefficient (ΔD) of <−0.6 $\mu m^2/s$ were defined as severely disrupted; the ones with 10−20% surface coverage of defects and −0.6 $\mu m^2/s < \Delta D < -0.3$ $\mu m^2/s$ as moderately disrupted; and the ones with 0−10% defect coverage and $\Delta D > -0.3$ $\mu m^2/s$ as negligibly disrupted. The color-coded "phase" diagram demonstrates the essence of our findings that amphiphilic Janus particles with increased hydrophobicity disrupt lipid bilayers more effectively. Their impact on the integrity of lipid bilayers is dependent on the particle concentration.

To further understand how the interaction between amphiphilic Janus particles and zwitterionic lipid bilayers change with varied particle hydrophobicity, we estimated the association rate constant (k_a) and activation energy (E_a) of particle adsorption on bilayers by using a previously reported method.[23] We imaged the adsorption of fluorescently labeled JPs on bilayers and measured the surface density of particles adsorbed as a function of time by using single-particle tracking (Figures 5a and S2). The values of k_a and E_a were obtained

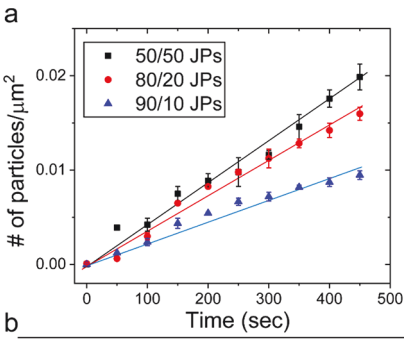

b

	k_a (M^{-1} s^{-1})	E_a (kJ/mol)
50/50 JPs	24700 ± 180	43.3 ± 0.02
80/20 JPs	13400 ± 120	44.8 ± 0.02
90/10 JPs	7900 ± 60	46.1 ± 0.02

Figure 5. (a) Number of Janus particles adsorbed on lipid bilayers as a function of time. The solid lines are linear fit to the corresponding data plots. Each data point is an average of the results from three images and the error bars represent standard deviation. (b) Association rate constant (k_a) and activation energy (E_a) of particle adsorption on lipid bilayers for different types of Janus particles.

after fitting the plots with the equations derived from the classical collision theory (see details in the Experimental Section). We found k_a (50/50 JPs) > k_a (80/20 JPs) > k_a (90/10 JPs) and a reverse relationship for E_a (Figure 5b). Given that the three types of amphiphilic Janus particles used in this study have similar surface coverage of positive charges, this result is a clear evidence that the hydrophobic interaction between amphiphilic Janus particles and lipid bilayers drives the adhesion of particles to the bilayers. This agrees with our observation in a recent study that amphiphilic Janus particles have significantly higher k_a than the positively charged particles without any hydrophobic groups. Amphiphilic Janus particles that are more hydrophobic are more effective in disrupting lipid bilayers. This is likely because they have stronger attraction to the bilayers and also because the larger surface coverage of their hydrophobic caps better extracts lipids from the intact bilayers after particle adhesion.

3. CONCLUSIONS

In this study, we investigated how amphiphilic JPs with varying hydrophobicities disrupt zwitterionic lipid membranes. The hydrophobicity of nanoparticles is a material property that can be challenging to quantify or control. We overcame this challenge by using chemical etching to control the surface area of the gold coating on Janus particles. As a result, we were able to control and measure the effective hydrophilic−lipophilic balance of these particles using the ratio of surface areas between the two sides. We showed that cationic/hydrophobic amphiphilic JPs induce lipid-depleted holes in zwitterionic lipid bilayers only when 20% or more of their particle surface is hydrophobic. Beyond this threshold, the larger the surface area of the hydrophobic portion of the particle, the more strongly

DOI: 10.1021/acs.langmuir.8b02298
Langmuir 2018, 34, 12387−12393

particles are attracted to the lipid bilayers and also, the lower the particle concentration needed for causing defects in the bilayers. When the hydrophobic area decreases below 10% of the total particle surface, amphiphilic JPs can no longer cause any visible defects in the bilayers. By measuring the association rate constant between the particles and lipid bilayers, we showed that the hydrophobic interactions between amphiphilic JPs and lipid bilayers are the main driving force for the adsorption of particles onto zwitterionic lipid bilayers and the depletion of lipids from the membrane. The lipid bilayers used in this study were formed on glass substrates, which are slightly negatively charged in water. The potential effect of the glass surface charge in the observed particle−membrane interactions is currently unclear. However, given that neither the 90/10 JPs nor the purely cationic nanoparticles caused membrane defects, the surface charge of the underlying glass surfaces is an unlikely cause for the particle-induced membrane defects. Nevertheless, a freestanding lipid membrane system would allow us to exclude the effect of the glass substrates in the interaction between particles and lipids in future studies.

We have shown previously that amphiphilic JPs disrupt lipid bilayers more effectively than uniform particles with the same mixture of chemical groups.[15] The new quantitative information provided by this study pinpoints the role of hydrophobicity in particle−membrane interactions. On the basis of our findings, many new questions that warrant future investigations arise. One such question is the effect of particle size. It is possible that particles of different sizes require different thresholds of particle concentration or surface coverage of hydrophobicity to induce defects in lipid membranes. Another potentially interesting area to explore is to decouple the effects of the Janus balance and particle hydrophobicity by varying the length of the hydrophobic alkyl chains on the particles. The Janus particle system is unique in that it allows systematic and quantitative investigations on the spatial arrangements of chemical groups on particle surfaces and affects their interactions with biological membranes.

4. EXPERIMENTAL SECTION

4.1. Materials and Reagents. Amine-functionalized silica particles (100 nm) were purchased from Nanocomposix (San Diego, CA). ODT was obtained from Sigma-Aldrich (St. Louis, MO). Chromium (99.99% purity) and gold (99.99% purity) pellets were purchased from Kurt J. Lesker (Jefferson Hills, PA). Cyanine5 *N*-hydroxysuccinimide ester (Cy5 NHS ester) was purchased from Lumiprobe Corporation (Hunt Valley, MD). Succinic anhydride (99% GC) was purchased from AK Scientific, Inc. (Union City, CA). Phospholipids, DOPC and 1,2-dipalmitoyl-*sn*-glycero-3-phosphoethanolamine-*N*-lissamine rhodamine B sulfonyl, were purchased from Avanti Polar Lipid (Alabaster, AL). *N*-(4,4-Difluoro-5,7-dimethyl-4-bora-3a,4a-diaza-*s*-indacene-3-propionyl)-1,2-dihexadecanoyl-*sn*-glycero-3-phosphoethanolamine, triethylammonium salt (BODIPY-DHPE) was purchased from Thermo Scientific (Waltham, MA). Potassium hexacyanoferrate(III), 98+% and potassium hexacyanoferrate(II) trihydrate, 98+% were obtained from Alfa Aesar (Haverhill, MA). Sodium thiosulfate anhydrous was purchased from MilliporeSigma (Burlington, MA). Potassium hydroxide was purchased from BDH Chemicals (Radnor, PA). Ultrapure water (resistivity of 18.2 MΩ·cm) was used for all experiments.

4.2. Methods. *4.2.1. Fabrication of Janus Particles.* To prepare cationic amphiphilic JPs (+/pho JPs), submonolayers of amine-modified silica nanoparticles were prepared using the solvent evaporation method with a slight modification.[24] Briefly, 50 μL of particles (0.1 wt % in ethanol) was cast on a piranha-cleaned glass microscope slide, and a continuous stream of the solution was used to reduce the coffee-ring effect. Subsequently, the submonolayers of particles were coated with thin films of chromium (5 nm in thickness) and then gold (25 nm) in an Edward Thermal evaporator (Nanoscale Characterization Facility at Indiana University). Immediately after metal deposition, the particle submonolayers on the glass microscope slides were immersed in ethanol containing 2 mM ODT. Prior to each experiment, the particles were sonicated off the microscope slides and rinsed in HCl−ethanol and then ethanol for three times each to remove the nonspecifically adsorbed ODT. The particle aggregates were further removed by differential centrifugation at 100 rcf for 30 s for three times and then 500 rcf for 30 s for three times. The particles were dispersed in DI water immediately before being added to supported lipid bilayers (SLBs).

To vary the Janus balance of amphiphilic particles by chemical etching, the Janus particles after metal deposition were immersed in a cyanide-based etching solution that was composed of 2.958 g Na_2SO_3, 0.051 g $K_4Fe^{II}(CN)_6$, 0.4002 g $K_3Fe^{III}(CN)_6$, and 6.72 g KOH in 180 mL of DI water. The etching time was varied as indicated in the text.

4.2.2. Fluorescent Labeling of Particles. Amine-modified silica nanoparticles were dispersed in 1× phosphate-buffered saline (PBS) (pH 7.4). Cy5 in DMSO (0.5 mg/mL) was added to the particle solution for the reaction. The final concentration of Cy5 was 0.8 μM and the particle concentration was 80 pM. After the reaction overnight at room temperature, the particles were washed with DI water and stored in ethanol.

4.2.3. Characterization of Particles. ZetaView nanoparticle tracking analyzer was used to measure the concentration of the Janus particles. Water contact angle measurements were done on the particle monolayers after ODT conjugation. SEM was used to characterize the morphology of the Janus particles. To measure the polar angle θ of the gold caps on Janus particles from the SEM images, the size of each gold cap on the particles was measured (as shown in Figure S3) and used to calculate the polar angle θ using the equation: $\theta = \arcsin(a/r)$, where a is the radii of the gold cap and r is the nanoparticle radii also measured in SEM images. The surface coverage of the gold cap on Janus particles was calculated using the equation: $A_{cap} = 2\pi r^2(1 - \cos\theta)$. For accurate measurements of θ from SEM, only particles that were oriented with their gold cap facing the SEM detector were selected.

4.2.4. Preparation of SLBs. Unilamellar vesicles of 100 nm were prepared using the extrusion method. Briefly, DOPC and Rhd-DHPE were mixed in a round-bottom flask at a 500:1 ratio in chloroform. The lipids were dried under nitrogen flow and then hydrated in 1× PBS to reach a final lipid concentration of 1 mg/mL. The hydrated lipid solution was frozen and thawed repeatedly for five times before being passed through a 100 nm filter membrane using a mini-extruder (Avanti Polar Lipids, Inc.). The SLBs were prepared by the vesicle fusion method. The lipid vesicles were diluted with 1× PBS to a final lipid concentration of 0.2 mg/mL and added to a precleaned glass-bottom imaging chamber. The lipid vesicles were incubated for 30 min. The quality of the lipid bilayers was checked under a fluorescence microscope after the incubation. Only the lipid bilayers with minimum immobilized lipid vesicles were used for the experiments. The excess lipid vesicles were rinsed away gently with DI water. The pH of the DI water was ≈6.6 under experimental conditions.

4.2.5. Fluorescence Imaging. Wide-field epifluorescence imaging was done with a Nikon Eclipse Ti microscope equipped with an Andor iXon3 EMCCD camera and a Nikon Plan Apo 100×/1.49 N.A. TIRF objective. All imaging experiments were done at room temperature. Each sample of lipid−particle interactions was repeated at least twice on different days to ensure reproducibility.

4.2.6. Fluorescence Recovery after Photobleaching. FRAP was measured using a Nikon Eclipse Ti microscope in an epifluorescence imaging mode. A circular region of the bilayer in a field of view was photobleached by a 562 nm laser at maximal intensity. After photobleaching, the fluorescence recovery of the bilayer was recorded for 4 min with 2 s intervals. In particle interaction experiments, FRAP of bilayers was measured before and 70 min after the addition of particles. The images were processed using "simFRAP", a built-in

DOI: 10.1021/acs.langmuir.8b02298
Langmuir 2018, 34, 12387−12393

plugin of ImageJ. Briefly, the diffusion coefficients were obtained by fitting the experimental FRAP data with a simulated recovery profile generated in this plugin.[25]

4.2.7. Measurement of Particle–Bilayer Binding Constant. Binding constants were determined by following a previous method based on a second-order binding process model.[23] Briefly, the adsorption of Cy5-labeled particles on the lipid bilayers was imaged using epifluorescence microscopy. A MATLAB single-particle tracking algorithm was used to count the number of adsorbed particles per unit surface area (N).[26] Assuming a second-order binding process between the particles and lipid bilayers, the overall adsorption rate, dN/dt, can then be expressed as

$$\frac{dN}{dt} = k_a C_s C_n \tag{1}$$

where k_a is the association rate constant, C_s is the maximum number of binding sites on the bilayer, and C_n is the bulk concentration of nanoparticles. By assuming a close packing of nanoparticles (d = 100 nm) on a flat surface, C_s was estimated to be 115. With known C_n and measured dN/dt, k_a was then calculated.

The activation energy (E_a) for adsorption was further calculated using the Arrhenius equation

$$E_a = [\ln(Q) - \ln(k_a)]k_B T \tag{2}$$

where Q is the diffusion collision frequency factor, k_B is the Boltzmann constant, and T is the temperature. Q was calculated using the following equation, based on the assumption that the particle–bilayer binding is limited by the diffusion of nanoparticles:

$$Q \approx 2000\pi R D N_a \tag{3}$$

where R is the radius of the collision sphere, equivalent to the radius of the nanoparticles (r) in our experimental system, and N_a is Avogadro's number. D is the diffusion coefficient of nanoparticles in bulk solution, obtained from the Stokes–Einstein equation

$$D = \frac{k_B T}{6\pi\eta r} \tag{4}$$

Q was estimated to be 9.285×10^{11} M^{-1} s^{-1} under our experimental conditions.

■ ASSOCIATED CONTENT

Supporting Information

The Supporting Information is available free of charge on the ACS Publications website at DOI: 10.1021/acs.langmuir.8b02298.

Water contact angle measurements for different types of Janus particles after chemical etching with or without ODT functionalization; zeta potential of Janus and uniform nanoparticles; SEM images showing the morphology of Janus particles at different etching times; fluorescence images showing the adsorption of Janus nanoparticles on lipid bilayers as a function of time; and SEM image showing Janus particles with their gold caps facing the detector (PDF)

■ AUTHOR INFORMATION

Corresponding Author

*E-mail: yy33@indiana.edu.

ORCID

Kwahun Lee: 0000-0003-4392-7466

Yan Yu: 0000-0001-6496-5045

Notes

The authors declare no competing financial interest.

■ ACKNOWLEDGMENTS

The authors thank Dr. Giovanni Gonzalez-Gutierrez at IUB Physical Biochemistry Instrumentation Facility, Dr. Jim Powers at IUB Light Microscopy Imaging Center, and Dr. Yi Yi at IUB Nanoscale Characterization Facility for assistance with instrument use. This work was supported by the National Science Foundation under grant no. 1705384.

■ REFERENCES

(1) Chen, J. M.; Hessler, J. A.; Putchakayala, K.; Panama, B. K.; Khan, D. P.; Hong, S.; Mullen, D. G.; DiMaggio, S. C.; Som, A.; Tew, G. N.; Lopatin, A. N.; Baker, J. R.; Holl, M. M. B.; Orr, B. G. Cationic Nanoparticles Induce Nanoscale Disruption in Living Cell Plasma Membranes. *J. Phys. Chem. B* **2009**, *113*, 11179–11185.

(2) Cho, E. C.; Xie, J.; Wurm, P. A.; Xia, Y. Understanding the Role of Surface Charges in Cellular Adsorption versus Internalization by Selectively Removing Gold Nanoparticles on the Cell Surface with a I-2/KI Etchant. *Nano Lett.* **2009**, *9*, 1080–1084.

(3) Arvizo, R. R.; Miranda, O. R.; Thompson, M. A.; Pabelick, C. M.; Bhattacharya, R.; Robertson, J. D.; Rotello, V. M.; Prakash, Y. S.; Mukherjee, P. Effect of Nanoparticle Surface Charge at the Plasma Membrane and Beyond. *Nano Lett.* **2010**, *10*, 2543–2548.

(4) Harush-Frenkel, O.; Rozentur, E.; Benita, S.; Altschuler, Y. Surface charge of nanoparticles determines their endocytic and transcytotic pathway in polarized MDCK cells. *Biomacromolecules* **2008**, *9*, 435–443.

(5) Hong, S.; Bielinska, A. U.; Mecke, A.; Keszler, B.; Beals, J. L.; Shi, X.; Balogh, L.; Orr, B. G.; Baker, J. R.; Holl, M. M. B. Interaction of poly(amidoamine) dendrimers with supported lipid bilayers and cells: Hole formation and the relation to transport. *Bioconjugate Chem.* **2004**, *15*, 774–782.

(6) Tatur, S.; Maccarini, M.; Barker, R.; Nelson, A.; Fragneto, G. Effect of Functionalized Gold Nanoparticles on Floating Lipid Bilayers. *Langmuir* **2013**, *29*, 6606–6614.

(7) Leroueil, P. R.; Berry, S. A.; Duthie, K.; Han, G.; Rotello, V. M.; McNerny, D. Q.; Baker, J. R.; Orr, B. G.; Holl, M. M. B. Wide varieties of cationic nanoparticles induce defects in supported lipid bilayers. *Nano Lett.* **2008**, *8*, 420–424.

(8) Jing, B.; Zhu, Y. Disruption of Supported Lipid Bilayers by Semihydrophobic Nanoparticles. *J. Am. Chem. Soc.* **2011**, *133*, 10983–10989.

(9) Van Lehn, R. C.; Ricci, M.; Silva, P. H. J.; Andreozzi, P.; Reguera, J.; Voitchovsky, K.; Stellacci, F.; Alexander-Katz, A. Lipid tail protrusions mediate the insertion of nanoparticles into model cell membranes. *Nat. Commun.* **2014**, *5*, 4482.

(10) Gao, J.; Zhang, O.; Ren, J.; Wu, C.; Zhao, Y. Aromaticity/Bulkiness of Surface Ligands to Promote the Interaction of Anionic Amphiphilic Gold Nanoparticles with Lipid Bilayers. *Langmuir* **2016**, *32*, 1601–1610.

(11) Jing, B.; Abot, R. C. T.; Zhu, Y. Semihydrophobic Nanoparticle-Induced Disruption of Supported Lipid Bilayers: Specific Ion Effect. *J. Phys. Chem. B* **2014**, *118*, 13175–13182.

(12) Shin, S. H. R.; Lee, H.-Y.; Bishop, K. J. M. Amphiphilic Nanoparticles Control the Growth and Stability of Lipid Bilayers with Open Edges. *Angew. Chem., Int. Ed.* **2015**, *54*, 10816–10820.

(13) Verma, A.; Uzun, O.; Hu, Y.; Hu, Y.; Han, H.-S.; Watson, N.; Chen, S.; Irvine, D. J.; Stellacci, F. Surface-structure-regulated cell-membrane penetration by monolayer-protected nanoparticles. *Nat. Mater.* **2008**, *7*, 588–595.

(14) Van Lehn, R. C.; Atukorale, P. U.; Carney, R. P.; Yang, Y.-S.; Stellacci, F.; Irvine, D. J.; Alexander-Katz, A. Effect of Particle Diameter and Surface Composition on the Spontaneous Fusion of Monolayer-Protected Gold Nanoparticles with Lipid Bilayers. *Nano Lett.* **2013**, *13*, 4060–4067.

(15) Lee, K.; Zhang, L.; Yi, Y.; Wang, X. Q.; Yu, Y. Rupture of Lipid Membranes Induced by Amphiphilic Janus Nanoparticles. *ACS Nano* **2018**, *12*, 3646–3657.

DOI: 10.1021/acs.langmuir.8b02298
Langmuir 2018, 34, 12387–12393

(16) Lee, W.; Cho, N.-J.; Xiong, A.; Glenn, J. S.; Frank, C. W. Hydrophobic nanoparticles improve permeability of cell-encapsulating poly(ethylene glycol) hydrogels while maintaining patternability. *Proc. Natl. Acad. Sci. U.S.A.* **2010**, *107*, 20709−20714.
(17) Andala, D. M.; Shin, S. H. R.; Lee, H.-Y.; Bishop, K. J. M. Templated Synthesis of Amphiphilic Nanoparticles at the Liquid-Liquid Interface. *ACS Nano* **2012**, *6*, 1044−1050.
(18) Lee, H.-Y.; Shin, S. H. R.; Abezgauz, L.; Lewis, S. A.; Chirsan, A. M.; Danino, D.; Bishop, K. J. M. Integration of Gold Nanoparticles into Bilayer Structures via Adaptive Surface Chemistry. *J. Am. Chem. Soc.* **2013**, *135*, 12476.
(19) Atukorale, P. U.; Yang, Y.-S.; Bekdemir, A.; Carney, R. P.; Silva, P. J.; Watson, N.; Stellacci, F.; Irvine, D. J. Influence of the glycocalyx and plasma membrane composition on amphiphilic gold nanoparticle association with erythrocytes. *Nanoscale* **2015**, *7*, 11420−11432.
(20) Bazant, M. Z.; Squires, T. M. Induced-charge electrokinetic phenomena. *Curr. Opin. Colloid Interface Sci.* **2010**, *15*, 203−213.
(21) Pincet, F.; Adrien, V.; Yang, R.; Delacotte, J.; Rothman, J. E.; Urbach, W.; Tareste, D. FRAP to Characterize Molecular Diffusion and Interaction in Various Membrane Environments. *PLoS One* **2016**, *11*, No. e0158457.
(22) Ladha, S.; Mackie, A. R.; Harvey, L. J.; Clark, D. C.; Lea, E. J.; Brullemans, M.; Duclohier, H. Lateral diffusion in planar lipid bilayers: a fluorescence recovery after photobleaching investigation of its modulation by lipid composition, cholesterol, or alamethicin content and divalent cations. *Biophys. J.* **1996**, *71*, 1364−1373.
(23) Wei, L.; Zhao, X.; Chen, B.; Li, H.; Xiao, L.; Yeung, E. S. Frozen translational and rotational motion of human immunodeficiency virus transacting activator of transcription peptide-modified nanocargo on neutral lipid bilayer. *Anal. Chem.* **2013**, *85*, 5169−5175.
(24) Lee, K.; Yu, Y. Janus nanoparticles for T cell activation: clustering ligands to enhance stimulation. *J. Mater. Chem. B* **2017**, *5*, 4410−4415.
(25) Blumenthal, D.; Goldstien, L.; Edidin, M.; Gheber, L. A. Universal Approach to FRAP Analysis of Arbitrary Bleaching Patterns. *Sci. Rep.* **2015**, *5*, 11655.
(26) Parthasarathy, R. Rapid, accurate particle tracking by calculation of radial symmetry centers. *Nat. Methods* **2012**, *9*, 724−726.

DOI: 10.1021/acs.langmuir.8b02298
Langmuir 2018, 34, 12387−12393